Excitons in one-phonon resonant Raman scattering: Deformation-potential interaction

A. Cantarero,* C. Trallero-Giner,† and M. Cardona
Max-Planck-Institut für Festkörperforschung, Heisenbergstrasse 1, Postfach 80 06 65, D-7000 Stuttgart 80, Federal Republic of Germany
(Received 8 November 1988)

A theory of one-phonon resonant Raman scattering in diamond and zinc-blende-type semiconductors which includes excitonic effects has been developed. The theory can be applied at frequencies below and above the band gap. We have considered the deformation-potential interaction for the electron–one-phonon coupling, and discrete and continuous exciton states have been taken as intermediate states in the process. The interband transitions between different valence bands (heavy and light holes and split-off bands) included in the calculation of the Raman tensor are characterized by excitonic states with different Bohr radii. General analytical expressions of the matrix elements corresponding to different transitions between excitonic states (discrete-discrete, discrete-continuous, and continuous-continuous) are reported as a function of the Bohr-radius ratio. A simplified expression of the Raman tensor obtained under the assumption of the same Bohr radii for both excitonic transitions is given. These results are used to calculate the absolute value of the Raman efficiency in the E_0 and $E_0+\Delta_0$ absorption edge of III-V compound semiconductors. Comparison with the electron-hole uncorrelated theory and with the corresponding experimental data recently reported for GaP, GaAs, and InP explains these spectra and emphasizes the decisive role of excitons in the one-phonon resonant Raman scattering.

I. INTRODUCTION

Raman scattering has proved to be a powerful technique in the study of elementary excitations in semiconductors as well as their interactions.[1] In particular, the study of excitons and their interactions with phonons has received some theoretical attention in the past.[2–5]

Since the work of Loudon,[6] only few papers have appeared on the theory of one-phonon Raman scattering including excitonic effects. Ganguly and Birman[3] calculated the Raman tensor including excitons as intermediate states (weak exciton-photon coupling) for deformation-potential (DP) and Fröhlich electron-phonon interactions, giving an explicit equation for the DP case. Martin[4] repeated the calculations of Ganguly with the Green-function formalism, whereby he studied only the region below the band gap. Zeyher *et al.*[5] calculated the first-order Raman tensor considering only one valence band and the corresponding continuum excitonic state. Later, in a similar way, Käräjämäki *et al.*[7] developed the theory of resonant Brillouin scattering for a three-band process, considering exciton states for the conduction, valence, and split-off bands. Trallero and Sotolongo[8] treated the hot-exciton problem, and then they studied the region above the band gap.

Recently, Raman experiments were performed in the proximity of the critical points (CP's) E_0 and $E_0+\Delta_0$ in several III-V compound semiconductors[9–12] as well as in ternary alloys such as $Al_xGa_{1-x}As$ (Refs. 13 and 14) and absolute values of Raman efficiency were obtained. The Raman theory considering uncorrelated electron-hole pairs (free–electron-hole–pair theory, FET) explains quantitatively the observed resonances in GaAs near the $E_0+\Delta_0$ CP.[10] Nevertheless, the resonant enhancement observed at E_0 in GaAs[11] and at E_0 and $E_0+\Delta_0$ in GaP (Ref. 9) in scattering configurations corresponding to DP interaction (both TO and LO phonons) is much stronger than the values reported by the FET. In the same way, unsatisfactory attempts to fit the experimental profile for resonant Raman scattering by LO phonons at $E_0+\Delta_0$ have been made in InP.[12]

These discrepancies were attributed to exciton effects and, in fact, some attempts were made to adapt (renormalize) Martin's calculations to the cases at hand and good agreement with the slope of the exciton peak in the region below the band gap was obtained.[11] However, it has not been possible, up to now, to explain the absolute values of resonant Raman efficiencies with a reliable theoretical model.

As already mentioned, the calculations of resonance effects including exciton interaction found in the literature are not sufficiently complete to allow generalization to other materials and critical points for which absolute values of Raman efficiencies have been measured. Hence the need for comprehensive studies of the Raman polarizability including excitonic effects. Here we perform such studies for the case in which deformation-potential interaction determines the scattering mechanism.

In the III-V compound semiconductors the fourfold-degenerate valence-band maximum leads to the existence of light and heavy holes and its twofold-degenerate spin-orbit-split component to split-off holes. The inclusion of Coulomb interaction between electrons and holes thus generates several exciton branches, in general with different Bohr radii. Here heavy, light, and split-off excitons will be taken into account using the Wannier-Mott exciton model (effective-mass approximation). In the allowed Raman scattering by LO and TO phonons several

excitonic intermediate states will thus be included. These aspects are discussed in Sec. II of this paper, where the Raman polarizability is calculated. Section III is devoted to the comparison of our calculations with experimental data of several III-V compounds. In Sec. IV the conclusions are summarized.

II. THEORY

The scattering efficiency per unit crystal length, and solid angle can be written as[6]

$$\frac{dS}{d\Omega}=\frac{\omega_s^3\omega_l}{c^4}\frac{\hbar}{2V_cM^*\omega_0}\frac{n_s}{n_l}[N(\omega_0)+1]\sum_i|\boldsymbol{\varepsilon}_s\cdot\overleftrightarrow{\mathbf{R}}_i\cdot\boldsymbol{\varepsilon}_l|^2 , \tag{1}$$

where V_c is the volume of the primitive cell, M^* the reduced mass of the atoms contributing to the optical mode, $N(\omega_0)$ the Bose-Einstein factor of the phonon, c the speed of light, and ω_0 the phonon frequency. In Eq. (1) n, ω, and $\boldsymbol{\varepsilon}$ are the refractive index and the frequency and polarization vector of the light. The indices l and s refer always to laser and scattered light, respectively. R_i are the three components of the Raman tensor for the zone-center optical phonons, in the case of zinc-blende and assuming propagation along the Cartesian axes:

$$R_x=\begin{bmatrix}0&0&0\\0&0&a\\0&a&0\end{bmatrix},\quad R_y=\begin{bmatrix}0&0&a\\0&0&0\\a&0&0\end{bmatrix},\quad R_z=\begin{bmatrix}0&a&0\\a&0&0\\0&0&0\end{bmatrix}. \tag{2}$$

The Raman polarizability a corresponding to a process of scattering of a photon by a phonon from initial state i to final state f is given by[3]

$$a=\frac{n_ln_s}{2\pi}\frac{V_c}{\bar{u}_0}\frac{1}{\hbar\omega_l}W_{fi}(\omega_s,\boldsymbol{\varepsilon}_s;\omega_l,\boldsymbol{\varepsilon}_l) , \tag{3}$$

where relative displacement $\bar{u}_0$ is defined as

$$\bar{u}_0=\left[\frac{\hbar V_c}{2VM^*\omega_0}\right]^{1/2} \tag{4}$$

and V is the volume of the crystal. W_{fi} is the amplitude probability corresponding to the scattering of a photon with the emission of an optical phonon.

For one-phonon resonant Raman scattering (OPRRS), the Raman efficiency is obtained from third-order perturbation theory. In the case in which excitons are taken as virtual intermediate states, and neglecting polariton effects, the matrix element W_{fi} can be written as a function of exciton-radiation (H_{ER}) and exciton-lattice (H_{EL}) interaction Hamiltonians as

$$W_{fi}=\sum_{p,q}\left[\frac{\langle f|H_{\mathrm{ER}}|q\rangle\langle q|H_{\mathrm{EL}}|p\rangle\langle p|H_{\mathrm{ER}}|i\rangle}{(\hbar\omega_l-E_p+i\Gamma_p)(\hbar\omega_s-E_q+i\Gamma_q)}+\frac{\langle f|H_{\mathrm{ER}}|p\rangle\langle p|H_{\mathrm{EL}}|q\rangle\langle q|H_{\mathrm{ER}}|i\rangle}{(\hbar\omega_l+E_q+i\Gamma_q)(\hbar\omega_s+E_p+i\Gamma_p)}\right] . \tag{5}$$

The indices p and q refer to excitonic intermediate states; E_α and Γ_α ($\alpha=p,q$) are their respective energies and lifetime broadenings.

The exciton-radiation and exciton-lattice interaction Hamiltonians can be expressed as[3]

$$H_{\mathrm{ER}}=\sum_{\substack{\mathbf{K},p,\\ \boldsymbol{\varepsilon},\boldsymbol{\kappa}}}\{T_{cv}^p(\mathbf{K})D_{p\mathbf{K}}^\dagger(a_{\boldsymbol{\kappa},\boldsymbol{\varepsilon}}+a_{-\boldsymbol{\kappa},\boldsymbol{\varepsilon}}^\dagger)+[T_{cv}^p(\mathbf{K})]^*D_{p\mathbf{K}}(a_{\boldsymbol{\kappa},\boldsymbol{\varepsilon}}+a_{-\boldsymbol{\kappa},\boldsymbol{\varepsilon}}^\dagger)\} ,$$
$$H_{\mathrm{EL}}=\sum_{\substack{\mathbf{Q},\nu,\\ p,q,\\ \mathbf{K},\mathbf{K}'}}S_{qp}^{\mathbf{K}'\mathbf{K}}(\mathbf{Q})D_{q\mathbf{K}'}^\dagger D_{p\mathbf{K}}(b_{\mathbf{Q},\nu}^\dagger+b_{-\mathbf{Q},\nu}) , \tag{6}$$

where $D_{p\mathbf{K}}$ ($D_{p\mathbf{K}}^\dagger$), $a_{\boldsymbol{\kappa},\boldsymbol{\varepsilon}}$ ($a_{-\boldsymbol{\kappa},\boldsymbol{\varepsilon}}^\dagger$), and $b_{-\mathbf{Q},\nu}$ ($b_{\mathbf{Q},\nu}^\dagger$) are annihilation (creation) operators for excitons, photons, and phonons, respectively, $\boldsymbol{\kappa}$ is the wave vector of the light, $\mathbf{Q}$ the quasimomentum of the phonon, ν represents the phonon branch, and $\mathbf{K}$ is the center-of-mass momentum of the exciton. The exciton-photon coupling constants T are given, for allowed transitions, by[15]

$$T_{cv}^p(\mathbf{K})=-\frac{e}{m}\left[\frac{2\pi\hbar}{\omega n^2}\right]^{1/2}\boldsymbol{\varepsilon}\cdot\langle c|\mathbf{p}|v\rangle\psi_p(0)\delta_{\mathbf{K},\boldsymbol{\kappa}} , \tag{7}$$

$\langle c|\mathbf{p}|v\rangle$ being the matrix element of the momentum operator and $\psi_p(\mathbf{r})$ the internal exciton wave function.

The exciton-phonon coupling constant can be expressed, for DP interaction, as[4]

$$S_{qp}^{\mathbf{K}'\mathbf{K}}(\mathbf{Q})=\frac{\bar{u}_0\sqrt{3}}{2a_0}[D_e^\nu(\mathbf{r})I_{qp}^h(\mathbf{Q})-D_h^\nu(\mathbf{r})I_{qp}^e(-\mathbf{Q})]\times\delta_{\mathbf{K}',\mathbf{K}+\mathbf{Q}} , \tag{8}$$

$D_\alpha^\nu(\mathbf{r})$ ($\alpha=e,h$) being the DP as defined by Bir and Pikus[16] and a_0 is the lattice constant. $I_{qp}^\alpha(\mathbf{Q})$ ($\alpha=e,h$) are equal to

$$I_{qp}^\alpha(\mathbf{Q})=\int d^3r\,\psi_q^*(\mathbf{r})\exp\left[-i\frac{m_\alpha}{m_e+m_h}\mathbf{Q}\cdot\mathbf{r}\right]\psi_p(\mathbf{r}) , \tag{9}$$

m_e and m_h being the effective masses for electrons and holes.

In an one-phonon process $\mathbf{Q}\approx0$ and Eq. (9) can be simplified to

$$I_{qp}=\int d^3r\,\psi_q^*(\mathbf{r})\psi_p(\mathbf{r}) . \tag{10}$$

Introducing expressions (5)–(8) into Eq. (2) and considering two excitonic bands p and q, i.e., a set of bands cv_p,cv_q, the contribution to the Raman polarizability can be written as

$$a_{qp}=\frac{a_0^2}{2m}\frac{R_H^2 a_H^3\sqrt{3}}{\hbar\omega_l(\hbar\omega_l\hbar\omega_s)^{1/2}}\left[\langle c|\mathbf{p}\cdot\boldsymbol{\varepsilon}_s|v_q\rangle\langle v_q|D_h^\nu|v_p\rangle\langle v_p|\mathbf{p}\cdot\boldsymbol{\varepsilon}_l|c\rangle\frac{\psi_q^*(0)I_{qp}\psi_p(0)}{(\hbar\omega_l-E_p+i\Gamma_p)(\hbar\omega_s-E_q+i\Gamma_q)}\right.$$
$$\left.+\langle c|\mathbf{p}\cdot\boldsymbol{\varepsilon}_s|v_p\rangle\langle v_p|D_h^\nu|v_q\rangle\langle v_q|\mathbf{p}\cdot\boldsymbol{\varepsilon}_l|c\rangle\frac{\psi_p^*(0)I_{pq}\psi_q(0)}{(\hbar\omega_l+E_q+i\Gamma_q)(\hbar\omega_s+E_p+i\Gamma_p)}\right], \quad (11)$$

where R_H and a_H are the rydberg and Bohr radius of the hydrogen atom.

Equation (11) is quite general, the only approximation being that involved in the choice of the envelope function. In the case in which it is taken to be a hydrogenic function one should keep in mind in Eq. (11) that the virtual exciton transitions take place from a p to a q band, with different Bohr radii. Thus it is necessary to know the tensorial component of the DP for the corresponding Bohr functions together with the matrix elements I_{pq}.

A. Matrix elements

The Wannier-Mott exciton wave functions for the discrete spectrum are taken to be (for the angular momentum $l=0$)[17]

$$\psi_{pm}(\rho)=\frac{1}{(\pi m^3 a_p^3)^{1/2}}e^{-\rho/m}F(1-m,2,2\rho/m), \quad (12)$$

with $E_m=E_g-R/m^2$, a_p being the Bohr radius of exciton p, $\boldsymbol{\rho}=\mathbf{r}/a_p$, $F(a,b,z)$ the confluent hypergeometric function, E_g the corresponding gap, and R the exciton rydberg. For the continuum states we have[17]

$$\psi_{pk}(\rho)=\frac{1}{\sqrt{\pi V}}ke^{\pi/2k}|\Gamma(1-i/k)|e^{-ik\rho}$$
$$\times F(1+i/k,2,2ik\rho), \quad (13)$$

with $E_k=E_g+Rk^2$, $\Gamma(z)$ the gamma function, and $\mu^{-1}=m_e^{-1}+m_h^{-1}$. The functions of Eq. (13) are normalized as follows:

$$\int_v \psi_{pk}^*(r)\psi_{pk'}(r)d^3r=2\pi\delta(k-k'). \quad (14)$$

1. Discrete-discrete matrix element

The matrix elements corresponding to a discrete-discrete transition are obtained by substituting Eq. (12) in Eq. (10) and using the expression (A2) of Appendix A:

$$I_{mn}=8(-1)^m(nm)^{5/2}f_{qp}^{3/2}(f_{qp}-1)\frac{(n-mf_{qp})^{m+n-3}}{(n+mf_{qp})^{m+n+1}}$$
$$\times F(1-m,1-n,2,-4nmf_{qp}/(n-mf_{qp})^2), \quad (15)$$

where $f_{qp}=a_q/a_p$ is the ratio of Bohr radii of final and initial states.

The matrix element between m and n states satisfies the property:

$$I_{mn}(f_{qp}^{-1})=I_{nm}(f_{qp}). \quad (16)$$

Figure 1 shows the matrix element as a function of the parameter f_{qp} for m,n from 1 to 3. The value of I_{mn} for f_{qp} larger than 1 can be obtained through Eq. (16). As we can see from Fig. 1, the matrix elements I_{mn}, in the special case when $f_{qp}=1$, are given by

$$I_{mn}(1)=\delta_{mn}. \quad (17)$$

The matrix elements I_{mn} $(m\neq n)$ can be larger than I_{mm} for same range of values of f_{qp} (see Fig. 1).

2. Discrete-continuous matrix element

The continuous-discrete and discrete-continuous matrix elements are complex conjugates of each other, thus we only calculate one of them.

By applying to Eq. (10) relation (A2), with the wave functions given by Eqs. (12) and (13), we obtain

$$I_{mk}(f_{qp})=\left[\frac{a_q^3}{V}\right]^{1/2}8\sqrt{2\pi}(-1)^m(f_{qp}-1)m^{5/2}\sqrt{k}\frac{\exp\left[-\frac{2}{k}\tan^{-1}(mkf_{qp})\right]}{(1-e^{-2\pi/k})^{1/2}(1+m^2k^2f_{qp}^2)^{m+1}}G(m,k), \quad (18)$$

where the function $G(m,k)$ is real (see Appendix A) and it is defined as

$$G(m,k)=(1-imkf_{qp})^{2m-2}F(1-m,1+i/k,2,-4imkf_{qp}/(1-imkf_{qp})^2). \quad (19)$$

Hence, the matrix element for the continuous-discrete and discrete-continuous transitions are the same. The following relations hold:

$$I_{km}(f_{qp})=I_{mk}(f_{qp}^{-1})=I_{km}^*(f_{qp}). \quad (20)$$

In the trivial case in which $f_{qp}=1$, the matrix element $I_{km}(1)=0$ as follows from the orthogonality of the continuous and the discrete spectra.

We have plotted in Fig. 2 the matrix elements I_{mk} [in units of $(a_q^3/V)^{1/2}$] as a function of k for two different values of f_{qp}. Only the cases $m=1,2$ have been considered in order to simplify the figure. The matrix elements are seen to decay rapidly with increasing m. We can also observe that of $f_{qp}\neq 0$, $a_q^{3/2}V^{-1/2}I_{mk}$ increases with f_{qp} for a fixed value of k, obtaining the limiting case

for $f_{qp}=0$:

$$\left[\frac{V}{a_q^3}\right]^{1/2} I_{mk}(0)=\frac{8(-1)^{m+1}(2\pi k)^{1/2}}{(1-e^{-2\pi/k})^{1/2}} . \tag{21}$$

3. *Continuous-continuous matrix element*

The matrix elements for the continuous-continuous case are also found to be, by using Eq. (A2),

$$I_{kk'}=-\frac{a_q^3}{V}\frac{16\pi\sqrt{kk'}(f_{qp}-1)e^{-\pi/k'}}{(1-e^{-2\pi/k})^{1/2}(1-e^{-2\pi/k'})^{1/2}} \times\frac{1}{(k'f_{qp}-k)(k'f_{qp}+k)^3}G(k,k') , \tag{22}$$

where, as in the continuous-discrete case, $G(k,k')$ is a real function (see Appendix A), in this case defined as

$$G(k,k')=\left[\frac{k'f_{qp}-k}{k'f_{qp}+k}\right]^{i/k'-i/k} F(1-i/k,1+i/k',2,4kk'f_{qp}/(k'f_{qp}+k)^2) . \tag{23}$$

When $f_{qp}\to 1$, the matrix element of Eq. (22) tends to the normalization condition given by Eq. (14). That can be shown by taking the assymptotic expansion of the wave function (Ref. 17 makes an exhaustive analysis of this problem).

Figure 3 shows the magnitude of $|I_{kk'}(f_{qp})|$, in units of $a_q^3V^{-1}$, for several values of f_{qp} [in order to obtain a graphic representation of Eq. (22) we added a small imaginary component to f_{qp}, i.e., $f_{qp}+i\varepsilon$, with $\varepsilon\to 0$]. As can be seen from Fig. 3, the matrix element is practically zero except in a small interval around $k=k'f_{qp}$. In fact, when $f_{qp}=1$ it is a delta function [see Eq. (14)]. We approximate in our calculations $I_{kk'}$ by a delta function with the corresponding normalization factor:

$$I_{kk'}\simeq\frac{a_q^3}{V}\frac{1}{(f_{qp})^{1/2}}\left[\frac{1-e^{-2\pi/k'f_{qp}}}{1-e^{-2\pi/k'}}\right]^{1/2} 2\pi\delta(k-k'f_{qp}) . \tag{24}$$

Figure 4 shows the strength of the matrix element as a function of k' for a fixed value of f_{qp} ($f_{qp}=1.1$). The

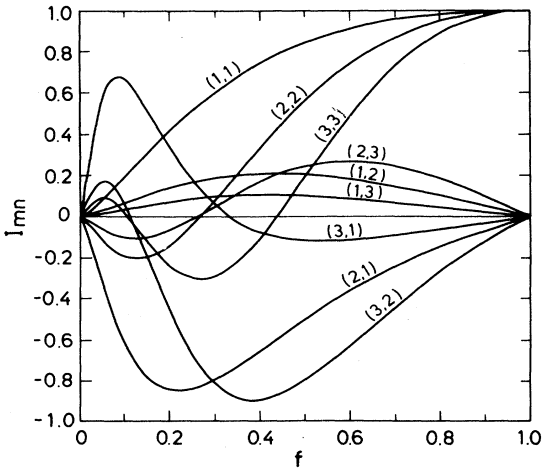

FIG. 1. Matrix elements I_{mn} as a function of f_{qp} for different values of m and n (from 1 to 3).

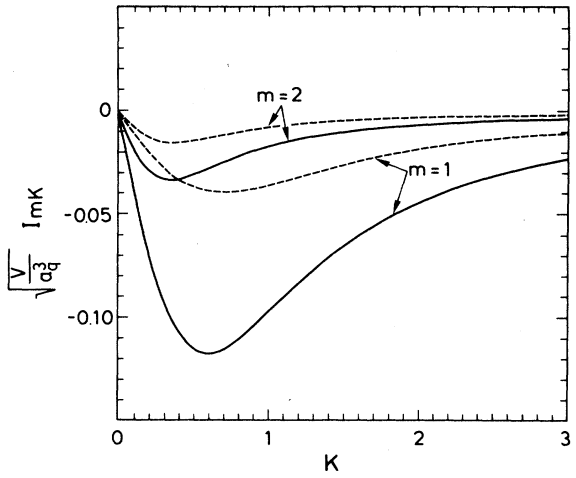

FIG. 2. Matrix elements $I_{mk}(Va_q^{-3})^{1/2}$ as a function of k for $m=1,2$ and two different values of f_{qp}: $f_{qp}=1.1$, dashed lines; $f_{qp}=1.5$, solid lines.

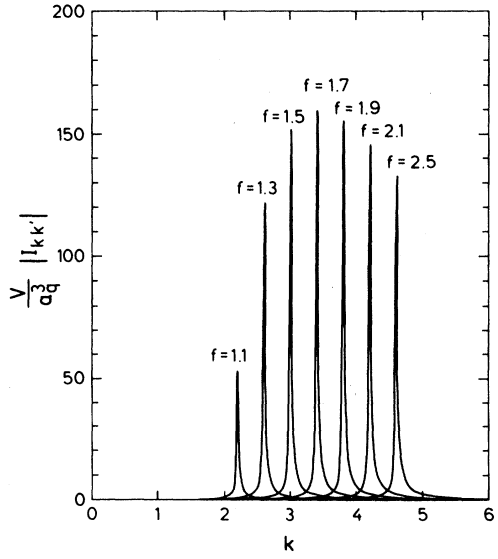

FIG. 3. The magnitude $|I_{kk'}|Va_q^{-3}$ ($k'=2$) as a function of k for several values of f_{qp} (from 1.1 to 2.5).

limiting values are

$$I_{kk'} \simeq \frac{a_q^3}{V} \frac{16\pi(f_{qp}-1)e^{-\pi/k}}{k^{7/2}(1-e^{-2\pi/k})^{1/2}} \sqrt{k'} \tag{25}$$

for $k' \to 0$ (it tends to zero as $\sqrt{k'}$) and

$$I_{kk'} \simeq -\frac{a_q^3}{V} \frac{16\sqrt{\pi k}\,(f_{qp}-1)}{\sqrt{2} f_{qp}^4 (1-e^{-2\pi/k})^{1/2}} \frac{e^{-\pi/k'}}{(k')^3} \tag{26}$$

for $k' \to \infty$ (it tends to zero as $e^{-\pi/k'}$). When both k and k' are zero, $I_{kk'}$ is obviously zero.

B. The Raman polarizability

The component a_{pq} of the Raman polarizability can be obtained by introducing the calculated matrix elements into Eq. (11):

$$\begin{aligned} a_{qp} = K_{qp} \Bigg[& \sum_{n,m=1}^{\infty} \frac{1}{(nm)^{3/2}} \frac{I_{mn}(f_{qp})}{[\eta_p + 1/n^2 + i\gamma_p(n)][\eta_q - \eta_{0q} + 1/m^2 + i\gamma_q(m)]} \\ & + \frac{1}{\sqrt{2\pi}} \sum_{m=1}^{\infty} \int_0^{\infty} dk \frac{\sqrt{k}}{(1-e^{-2\pi/k})^{1/2}} \Bigg[\frac{I_{mk}(f_{qp})(Va_q^{-3})^{1/2}}{[\eta_p - k^2 + i\gamma_p(k)][\eta_q - \eta_{0q} + 1/m^2 + i\gamma_q(m)]} \\ & + \frac{I_{mk}(f_{pq}^{-1})(Va_p^{-3})^{1/2}}{[\eta_p + 1/m^2 + i\gamma_p(m)][\eta_q - \eta_{0q} - k^2 + i\gamma_q(k)]} \Bigg] \\ & + \int_0^{\infty} dk \frac{k}{1-e^{-2\pi/k}} \frac{f_{qp}^{3/2}}{[\eta_p - k^2 + i\gamma_p(k)][\eta_q - \eta_{0q} - k^2 f_{qp}^2 + i\gamma_q(k)]} \Bigg], \end{aligned} \tag{27}$$

where $\eta_p = (\hbar\omega_l - E_{gp})/R_p$, E_{gp} being the gap related to exciton p and $\eta_{0p} = \hbar\omega_0/R_p$, and the lifetime broadening $\gamma_p = \Gamma_p/R_p$. The factor K_{qp} given in Eq. (27) is

$$K_{qp} = \frac{a_0^2}{2\pi m} \frac{R_H^2}{R_p R_q} \frac{a_H^3 \sqrt{3}}{(a_p a_q)^{3/2}} \times \frac{\langle c|\mathbf{p}\cdot\boldsymbol{\varepsilon}_s|v_q\rangle\langle v_q|D_h|v_p\rangle\langle v_p|\mathbf{p}\cdot\boldsymbol{\varepsilon}_l|c\rangle}{\hbar\omega_l(\hbar\omega_l\hbar\omega_s)^{1/2}} . \tag{28}$$

The first term on the right-hand side in Eq. (27) corresponds to the discrete-discrete excitonic transition, the second and the third to continuous-discrete and discrete-continuous contributions, and the last one to the continuous-continuous contribution. The integration over k in the continuous-continuous case can be performed as in Ref. 18.

The f_{qp} factor in the denominator of the continuous-continuous case arises from the simplification mentioned before. If the exact calculation is made, kf_{qp} must be substituted by k', the integrand multiplied by $I_{kk'}$ [Eq. (22)], and the integration extended to k'. Equation (27) was used in our calculations.

With the help of Eqs. (14) and (17), and the orthonormality of the discrete and continuous matrix elements in the case $f_{qp}=1$, Eq. (27) is then simplified to

$$\begin{aligned} a_{qp} = K_{qp} \Bigg[& \sum_{n=1}^{\infty} \frac{1}{n^3} \frac{1}{[\eta_p + 1/n^2 + i\gamma_p(n)][\eta_q - \eta_{0q} + 1/n^2 + i\gamma_q(n)]} \\ & - \tfrac{1}{2} \sum_{n=1}^{\infty} \frac{1}{n^3} \frac{1}{[\eta_p + 1/n^2 + i\gamma_p(k)][\eta_q - \eta_{0q} + 1/n^2 + i\gamma_q(k)]} \\ & + \frac{1}{4} \frac{1}{\eta_p - \eta_q + \eta_{0q} + i[\gamma_p(k) - \gamma_q(k)]} \\ & \times \left\{ \ln\left[\frac{\eta_q - \eta_{0q} + i\gamma_q(k)}{\eta_p + i\gamma_p(k)} \right] + \pi i \left[\coth\left[\frac{\pi}{[\eta_p + i\gamma_p(k)]^{1/2}} \right] - \coth\left[\frac{\pi}{[\eta_q - \eta_{0q} + i\gamma_q(k)]^{1/2}} \right] \right] \right\} \Bigg] \end{aligned} \tag{29}$$

with the assumption that $\gamma_p(k)$ and $\gamma_q(k)$ are constants. Figure 5 shows $|a_{qp}|^2$ for different values of the parameter f_{qp} ($f_{qp}=\frac{1}{2}$, 1, and 2) for the case $\eta_p=\eta_q=\eta$ and $\eta_{0q}=5$. The squared magnitude of the different contributions (discrete-discrete, discrete-continuous +continuous-discrete, and continuous-continuous) are also shown in Fig. 5. It can be seen in Fig. 5 that transitions between discrete and continuous states are important for $f_{qp} \neq 1$, in such a way that the larger contribution corresponds to frequencies close to incoming resonance when $f_{qp} < 1$ and close to outgoing resonance when $f_{qp} > 1$. It can also be observed that the continuous-continuous contribution increases when f_{qp} increases and it becomes even more important than the discrete-

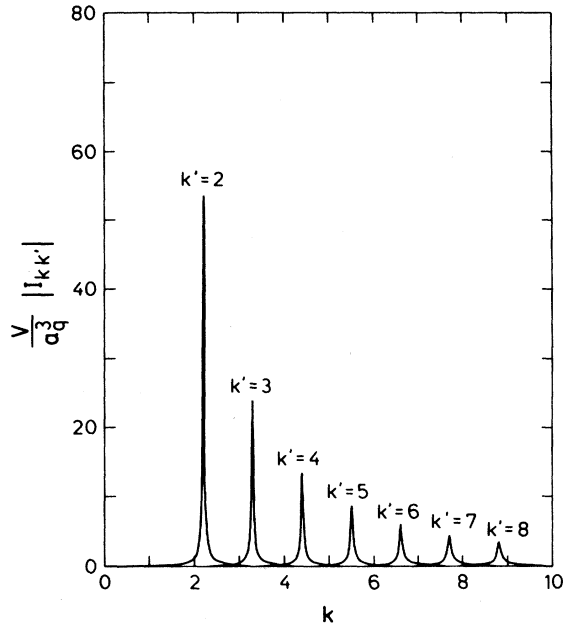

FIG. 4. The magnitude $|I_{kk'}|Va_q^{-3}$ ($f_{qp}=1.1$) as a function of k for several values of k' (from 2 to 8).

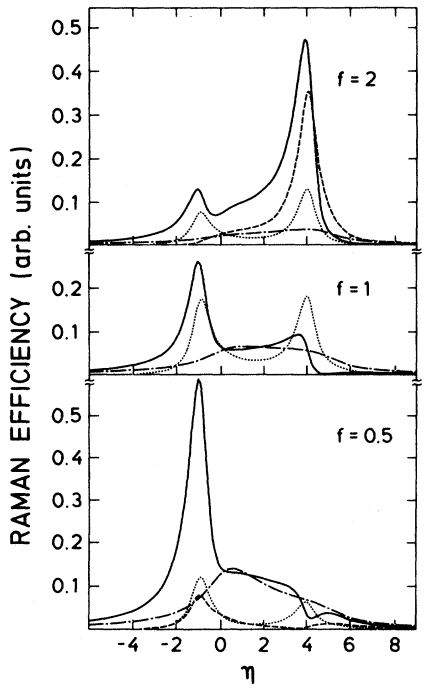

FIG. 5. Raman polarizability $|\alpha_{qp}|^2$ as a function of the parameter $\eta=(\hbar\omega_l-E_g)/R_{\rm lh}$ for three different values of f_{qp} (0.5, 1, and 2): solid lines. Also, the different contributions, discrete-discrete (short-dashed line), discrete-continuous (long-dashed line), and continuous-continuous (dot-dashed line) are shown in the figure).

discrete contribution, a consequence of the functional dependence of Eq. (27) on the parameter f_{qp}. Thus, for a small value of f_{qp}, $|\alpha_{qp}|^2$ is larger for outgoing resonances than for incoming ones, and the situation reverses when f_{qp} is close to or more than 1. Nevertheless, when the inverse diagram is also allowed ($q\rightarrow p$) and f_{qp} is not very different from 1, the value of α_{qp} obtained by adding both diagrams differs very little from the one obtained multiplying by 2 the diagram for $f_{qp}=1$ (it differs only very near resonance). In practice, if both diagrams are possible, one can use Eq. (29) instead of Eq. (27), which enormously simplifies the calculations.

III. APPLICATION TO III-V COMPOUNDS

In III-V compounds, in the vicinity of the E_0 and $E_0+\Delta_0$ CP's, three different sets of excitons are going to be formed between the conduction band and the three valence bands $|\frac{3}{2},\pm\frac{3}{2}\rangle$, $|\frac{3}{2},\pm\frac{1}{2}\rangle$, and $|\frac{1}{2},\pm\frac{1}{2}\rangle$, corresponding to hh, lh, and so. Then, eight diagrams will contribute to the resonance: lh$\rightarrow$lh, lh$\rightarrow$hh, lh$\rightarrow$s.o., hh$\rightarrow$lh, hh$\rightarrow$hh, hh$\rightarrow$s.o., s.o.$\rightarrow$lh, and s.o.$\rightarrow$hh (s.o.$\rightarrow$s.o. is zero by symmetry). The total Raman polarizability will be

$$\alpha=\sum_{p,q}\alpha_{qp}+b\ , \tag{30}$$

where $p,q=$lh, hh, s.o. and b is due to nonresonant terms.

The Γ_8 bands of III-V compounds are not spherically symmetric and the coefficients K_{qp} given by Eq. (30) will be different for the different diagrams. Instead of the matrix elements $\langle c|\mathbf{p}\cdot\boldsymbol{\epsilon}_s|v_q\rangle$, $\langle v_q|D_h^\gamma|v_p\rangle$, $\langle v_p|\mathbf{p}\cdot\boldsymbol{\epsilon}_l|c\rangle$ we took their mean value calculated for the star of the three fundamental directions of $\mathbf{k}$ space (see Appendix B).

In III-V compound semiconductors at the Γ_8 point the heavy- and light-hole valence bands are degenerate and the relative and translational motions of the exciton cannot be separated in the Schrödinger equation when Coulomb interaction is included in the Luttinger-Kohn Hamiltonian. Kane[19] has shown that it is possible to speak about two independent Wannier-Mott excitons with two different Bohr radii (heavy and light excitons) when the corresponding kinetic energy is larger than the exciton binding energy (larger center-of-mass exciton momentum). For calculating the matrix elements I_{qp} we need not the energy, but the wave function, for $\mathbf{K}\approx\mathbf{0}$. In order to simplify the problem we assume independent excitons with the same mean Bohr radius $\tilde{a}$ for the lh and hh excitons and a different one $a_{\rm s.o.}$ for the s.o. case.

The theory just described has been tested in several III-V compounds using as adjustable parameters only the Bohr radii and the lifetimes. The adjustment was performed by using a measured absolute value of α. Unfortunately, only GaP has been measured in the whole range around E_0 and $E_0+\Delta_0$. We also tried to fit GaAs and InP, the first one measured around E_0 and the second around $E_0+\Delta_0$.

The following empirical relation was used for the lifetimes:

$$\Gamma_p(n)=\Gamma_p(k)-[\Gamma_p(k)-\Gamma_p(1)]/n^2\ . \tag{31}$$

In all cases we took $\Gamma_p(k)=10$ meV. A background b related to nonresonant terms was added.

A. Gallium phosphide

The GaP is the only semiconductor for which absolute values of the Raman polarizability have been measured in a large frequency range including excitonic resonances.[9]

Figure 6 shows the experimental data taken from Ref. 9 and the fit with Eq. (27) (solid curve). The energies R_{hh}, R_{lh}, and $R_{s.o.}$ have been taken to be equal to the experimental rydbergs in E_0 and $E_0+\Delta_0$, respectively.[20] The parameters used in the fitting are summarized in Table I.

The dashed line in Fig. 6 corresponds to the calculation for uncorrelated electrons [Eq. (2) of Ref. 11, as calculated with the parameters used in Ref. 9]. The exciton energy, 1.503 eV, was chosen to coincide with that of the observed maximum, it agrees well with that obtained in reflectance measurements.[21]

The two main peaks of Fig. 6 correspond to the incoming and outgoing resonances with E_0, and the two minima (at 2.945 and 2.995 eV) to incoming and outgoing resonance with $E_0+\Delta_0$. The lifetimes were taken from experimental data for E_0 and to give the best slope near $E_0+\Delta_0$. The background was used to fit the high-energy region.

The absence of peaks at $E_0+\Delta_0$ is due to interference between different diagrams. It is interesting to note that the Bohr radius for the split-off exciton (54 Å) is very close to that obtained from the experimental rydberg in $E_0+\Delta_0$ (60 Å), and the Bohr radius $\bar{a}$ needed in E_0 (46 Å) is only about 20% away from the one obtained from R_{lh}. This proves that the approximation of taking only two Bohr radii is satisfactory and a more complicated band scheme unnecessary.

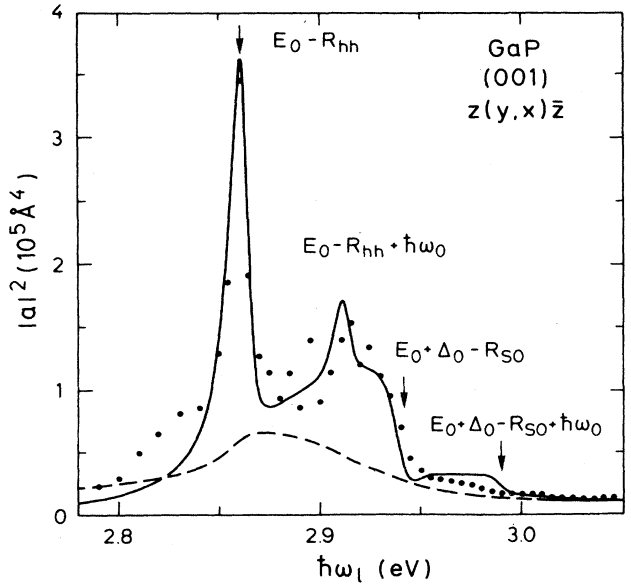

FIG. 6. Comparison with experimental data for GaP (Ref. 28). The dots represent the experimental points, the solid line the fit with Eq. (27), and the dashed line the best fit with a noncorrelated electron-hole–pair theory.

TABLE I. Numerical values of the parameters used for the theoretical fit of Fig. 6.

Parameter	Value	Ref.
R_{lh}	11 meV	20
$R_{s.o.}$	10 meV	20
E_0	2.873 eV	9
Δ_0	80 meV	21
$\hbar\omega_0$	50 meV	9
a_0	5.45 Å	25
d_0	47 eV	26
p^2/m	10.58 eV	a
Γ_{lh}	6 meV	
Γ_{hh}	5 meV	
$\Gamma_{s.o.}$	10 meV	
$\bar{a}$	46 Å	fit
$a_{s.o.}$	54 Å	fit
b	55 Å^2	fit

[a]This value was calculated from the expression (Ref. 18) $p^2/m=\frac{1}{2}(m/m_e-1)[E_0(E_0+\Delta_0)/E_0+\frac{2}{3}\Delta_0]$ for $m_e=0.12m_0$ (Ref. 9).

B. Gallium arsenide

Resonant Raman experiments for GaAs were presented in Ref. 11. The authors took measurements in several backscattering configurations, obtaining the Raman polarizability for the case of LO and TO phonons in two different samples.

We discuss here the results for the TO phonons, those for LO phonons being only slightly higher due to electro-optic contributions. As in the case of GaP, R_{lh} and R_{hh} were chosen to be equal to the experimental rydberg at E_0. For the s.o. rydberg we took the calculated one (80 Å).

The theoretical fit obtained with the parameters of Table II is presented in Fig. 7. Although the split-off energy is large for GaAs (340 meV), we used in the calculations all the diagrams used for GaP. The dashed line in Fig. 7 corresponds to the best fit with the free-electron–hole theory.[11] The discrepancy between $\bar{a}$ and the one obtained from the experimental rydberg is 40% instead of 20% found for GaP. This discrepancy may be related to the large luminescence existing at the E_0 CP

TABLE II. Numerical values of the parameters used for the theoretical fit of Fig. 7.

Parameter	Value	Ref.
R_{lh}	4.2 meV	27
$R_{s.o.}$	3.8 meV	calc.
E_0	1.506 eV	11
Δ_0	340 meV	11
$\hbar\omega_0$	33.7 meV	11
a_0	5.65 Å	11
d_0	44 eV	26
p^2/m	12.9 eV	11
Γ_{lh}	2.5 meV	
Γ_{hh}	2.5 meV	
$\Gamma_{s.o.}$	5 meV	11
$\bar{a}$	68 Å	fit
$a_{s.o.}$	80 Å	calc.
b	−670 Å^2	fit

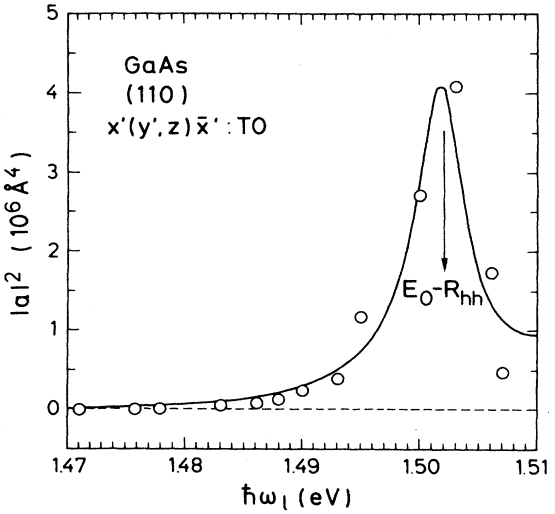

FIG. 7. Comparison of the theory with the experimental data for GaAs (Ref. 28). The dots correspond to the data as taken from Ref. 11, the solid line to our theory [Eq. (27)], and the dashed line was calculated with Eq. (2) of Ref. 11.

due to the fact that GaAs is a direct-band-gap semiconductor. The large background needed to fit the experimental data also points in this direction. The lifetimes are greater (less broadening) than for GaP; the latter is an indirect-band-gap semiconductor and direct excitons have plenty of channels to scatter into.

C. Indium phosphide

Indium phosphide has been measured[12] in the same scattering configuration as GaP in the region around $E_0+\Delta_0$. There are only a few experimental points; hence the fit was done with the calculated Bohr radii adding a small adjustable background. Figure 8 shows the fit obtained with the parameters of Table III. The value used for the DP constant d_0 is 35 eV, namely that calculated by the empirical pseudopotential method (EPM).[22] As in the case of GaP, the strong resonance tail observed at

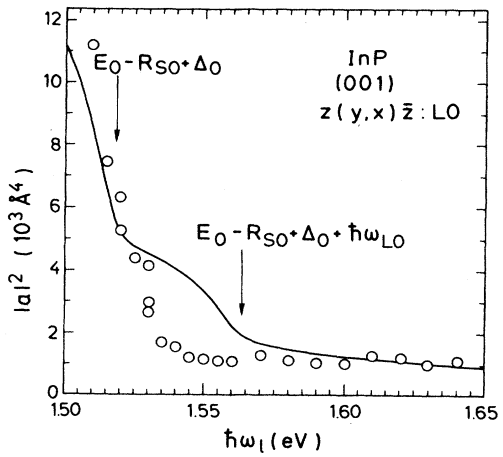

FIG. 8. Comparison with the experiment for InP (Ref. 28). The dots correspond to the data from Ref. 12 and the solid line to the values calculated with Eq. (27).

TABLE III. Numerical values of the parameters used for the theoretical fit of Fig. 8.

Parameter	Value	Ref.
R_{lh}	5.1 meV	12
$R_{s.o.}$	4.6 meV	calc.
E_0	1.415 eV	12
Δ_0	108 meV	12
$\hbar\omega_0$	43 meV	12
a_0	5.87 Å	12
d_0	35 eV	12
p^2/m	8.8 eV	12
Γ_{lh}	5 meV	12
Γ_{hh}	5 meV	12
$\Gamma_{s.o.}$	10 meV	
$\bar{a}$	115 Å	calc.
$a_{s.o.}$	130 Å	calc.
b	20 Å^2	fit

lower energy in the region near the $E_0+\Delta_0$ CP ($\hbar\omega_l < 1.55$ eV for InP and $\hbar\omega_l < 2.95$ eV for GaP) is due to excitonic effects.

IV. CONCLUSIONS

Raman polarizability for OPRRS is calculated for DP interaction including electron-hole correlation in the hydrogenic approximation. Several excitons related to different CP's are introduced, taking a different Bohr radius for each wave-function set. An explicit general expression valid to describe RRS experiments around E_0 and $E_0+\Delta_0$ in zinc-blende-type semiconductors is given for the Raman polarizability. A simplified expression for the case in which the exciton Bohr radii are equal is presented.

A comparison of our calculations with recent measurements is made, in absolute units, for GaP, GaAs, and InP. The good agreement between the theoretical and experimental data, and the comparison with the theory for uncorrelated electron-hole pairs clarify the role of excitons in III-V compounds and explain the observed spectral behavior in GaP, GaAs, and InP. The particular case of InP, in which only the broadenings are fitted, allows us to use a $d_0=35$ eV for the DP optical constant.

The theory can also be extended to direct allowed transitions in other semiconductors.

APPENDIX A

All the matrix elements between discrete-discrete, discrete-continuous, and continuous-continuous exciton states are integrals of the type

$$J(\alpha,\alpha')=\int_0^\infty e^{-(\lambda+\lambda')r/2} r^2 F(\alpha,2,\lambda r) \times F(\alpha',2,\lambda' r)\,dr \ . \tag{A1}$$

The evaluation of these integrals yields[17,23]

$$J(\alpha,\alpha')=16(-1)^\alpha[\lambda(1-\alpha)-\lambda'(1-\alpha')] \times\frac{(\lambda+\lambda')^{\alpha+\alpha'-3}}{(\lambda-\lambda')^{\alpha+\alpha'+1}} \times F(\alpha,\alpha',2,-4\lambda\lambda'/(\lambda-\lambda')^2) \ , \tag{A2}$$

where α is either $1-n$ or $1+i/k$ and $\lambda=2/k$ (or $2f/k$) or $2ik$ (or $2ikf$) in the discrete and continuous cases, respectively.

For the discrete-continuous case [Eq. (19)] the following function is obtained:

$$G(m,k)=(1-imkf)^{2(m-1)} \times F(1-m,1+i/k,2,-4imkf/(1-imkf)^2) , \quad \text{(A3)}$$

which is real, as can be shown by means of the first Kummer's relation[24]

$$F(a,b,c;z)=(1-z)^{-a}F(a,c-b,c,z/(z-1)) . \quad \text{(A4)}$$

From (A4) follows

$$(1-imkf)^{2(m-1)}F(1-m,1+i/k,2,-4imkf/(1-imkf)^2) =(1+imkf)^{2(m-1)}F(1-m,1-i/k,2,4imkf/(1+imkf)^2) , \quad \text{(A5)}$$

then $G(m,k)=G^*(m,k)$ and $G(m,k)$ is a real function.

The function $G(k,k')$ appearing in the continuous-continuous matrix element [Eq. (23)] is also real. The first solution of the hypergeometric equation also yields

$$F(a,b,c;z)=(1-z)^{c-a-b}F(c-a,c-b,c;z) . \quad \text{(A6)}$$

Applying (A6) to Eq. (23),

$$\left[\frac{k'f-k}{k'f+k}\right]^{i/k'-i/k} F(1-i/k,1+i/k',2,4kk'f/(k'f+k)^2) = \left[\frac{k'f-k}{k'f+k}\right]^{i/k-i/k'} F(1-i/k',1+i/k,2,4kk'f/(k'f+k)^2) , \quad \text{(A7)}$$

$G(k,k')=G^*(k,k')$ being real.

APPENDIX B

The valence bands are not spherically symmetric around Γ_8 in the III-V compounds and the quantity

$$\langle c|\mathbf{p}\cdot\boldsymbol{\varepsilon}_s|v_p\rangle\langle v_p|D_h|v_q\rangle\langle v_q|\mathbf{p}\cdot\boldsymbol{\varepsilon}_l|c\rangle \quad \text{(B1)}$$

depends on the direction of the $\mathbf{k}$ vector. In order to estimate the mean value of this quantity we made the calculation for a specific polarization direction $z(xy)\bar{z}$, without loss of generality. In that case, the matrix representation of D_h is

$$D_h=d_0\begin{bmatrix}0&1&0\\1&0&0\\0&0&0\end{bmatrix} \quad \text{(B2)}$$

and only the p_x and p_y components are different from zero. In (B2), d_0 is the DP optical constant. The wave functions can be represented as

$$\begin{aligned}
v_{\mathrm{hh}}^{+}&=|\tfrac{3}{2},\tfrac{3}{2}\rangle=\frac{1}{\sqrt{2}}(x+iy)\uparrow ,\\
v_{\mathrm{hh}}^{-}&=|\tfrac{3}{2},\tfrac{3}{2}\rangle=\frac{1}{\sqrt{2}}(x-iy)\downarrow ,\\
v_{\mathrm{lh}}^{+}&=|\tfrac{3}{2},\tfrac{1}{2}\rangle=\frac{1}{\sqrt{6}}(x+iy)\downarrow-(\tfrac{2}{3})^{1/2}z\uparrow ,\\
v_{\mathrm{lh}}^{-}&=|\tfrac{3}{2},-\tfrac{1}{2}\rangle=\frac{1}{\sqrt{6}}(x-iy)\uparrow+(\tfrac{2}{3})^{1/2}z\downarrow ,\\
v_{\mathrm{s.o.}}^{+}&=|\tfrac{1}{2},\tfrac{1}{2}\rangle=\frac{1}{\sqrt{3}}(x+iy)\downarrow+\frac{1}{\sqrt{3}}z\uparrow ,\\
v_{\mathrm{s.o.}}^{-}&=|\tfrac{1}{2},-\tfrac{1}{2}\rangle=\frac{1}{\sqrt{3}}(x-iy)\uparrow-\frac{1}{\sqrt{3}}z\downarrow .
\end{aligned} \quad \text{(B3)}$$

TABLE IV. Mean values of $\tilde{C}_{p\to q}$ in the mean directions of the (BZ) in the transitions involved in the vicinity of E_0 and $E_0+\Delta_0$ CP's.

Direction \ Transition	lh→lh	lh→hh	lh→s.o.	hh→hh	hh→lh	hh→s.o.	s.o.→lh	s.o.→hh
[001]	0	$\frac{1}{3}$	0	0	$\frac{1}{3}$	$\frac{2}{3}$	0	$\frac{2}{3}$
[100]	0	$\frac{2}{3}$	$\frac{2}{3}$	0	0	0	$\frac{1}{3}$	$\frac{1}{3}$
[010]	0	0	$\frac{1}{3}$	0	$\frac{2}{3}$	$\frac{1}{3}$	$\frac{2}{3}$	0
[110]	$\frac{1}{4}$	$\frac{1}{12}$	$\frac{1}{2}$	$\frac{1}{4}$	$\frac{1}{12}$	$\frac{1}{6}$	$\frac{1}{2}$	$\frac{1}{6}$
[011]	0	$\frac{1}{6}$	$\frac{1}{6}$	0	$\frac{1}{2}$	$\frac{1}{2}$	$\frac{1}{3}$	$\frac{1}{3}$
[101]	0	$\frac{1}{2}$	$\frac{1}{3}$	0	$\frac{1}{6}$	$\frac{1}{3}$	$\frac{1}{6}$	$\frac{1}{2}$
[111]	$\frac{1}{9}$	$\frac{2}{9}$	$\frac{1}{3}$	$\frac{1}{9}$	$\frac{2}{9}$	$\frac{1}{3}$	$\frac{1}{3}$	$\frac{1}{3}$
$\tilde{C}_{p\to q}$	$\frac{17}{18}\simeq\frac{1}{5}$	$\frac{61}{78}\simeq\frac{4}{5}$	1	$\frac{17}{78}\simeq\frac{1}{5}$	$\frac{61}{78}\simeq\frac{4}{5}$	1	1	1

In order to perform the k average we evaluated the contribution to the scattering of electrons along the "principal" directions of the Brillouin zone (BZ), namely, Λ, Δ, and Σ. We define $P=\langle s|p_x|x\rangle$.

Table IV shows the mean values:

$$\tilde{C}_{p\to q}\equiv\frac{3}{d_0}|P|^2\overline{\langle c|p_y|v_q\rangle\langle v_q|D_h^z|v_p\rangle\langle v_p|p_x|c\rangle}$$

for the different diagrams in the region about E_0 and $E_0+\Delta_0$ calculated in the principal directions. As we can see, these mean values are different from 1 only when transitions inside Γ_8 bands are considered. If a configuration in which a TO phonon is allowed is considered, we can repeat the calculations and obtain a slightly different result due to the fact that we did not integrate over the whole BZ, but only took the Λ, Δ, and Σ directions. The values obtained in that case are $\frac{61}{312}$ for the intraband terms and $\frac{215}{312}$ for interband (in the Γ_8 bands) terms, there being a 2% difference between the LO and TO values, a fact which confirms the correctness of taking only principal directions.

ACKNOWLEDGMENTS

Two of the authors (A.C. and C.T.-G.) thank the Generalitat Valenciana (Spain) and the Alexander von Humboldt Foundation (Federal Republic of Germany), respectively, for financial support.

*On leave from Departament de Física Aplicada, Universitat de València, E-46100 València, Spain.

†On leave from Department of Theoretical Physics, Havana University, Havana, Cuba.

[1]M. Cardona, in *Light Scattering in Solids II,* Vol. 50 of *Topics in Applied Physics,* edited by M. Cardona and G. Güntherodt (Springer, Heidelberg, 1982), p. 19.

[2]*Excitons,* Vol. 14 of *Topics in Current Physics,* edited by K. Cho (Springer, Heidelberg, 1979).

[3]A. K. Ganguly and J. L. Birman, Phys. Rev. **162**, 806 (1967).

[4]R. M. Martin, Phys. Rev. B **4**, 3676 (1971).

[5]R. Zeyher, Chiu-Sen Ting, and J. L. Birman, Phys. Rev. B **10**, 1725 (1974).

[6]R. Loudon, Adv. Phys. **13**, 423 (1964).

[7]E. Käräjämäki, R. Laiho, T. Levola, B. H. Bairamov, A. V. Gol'tsev, and T. Toporo, Phys. Rev. B **29**, 4508 (1984).

[8]C. Trallero and O. Sotolongo, Phys. Status Solidi B **127**, 121 (1985).

[9]W. Kauschke, V. Vorliček, and M. Cardona, Phys. Rev. B **36**, 9129 (1987).

[10]J. Menéndez and M. Cardona, Phys. Rev. B **31**, 3696 (1985).

[11]A. K. Sood, W. Kauschke, J. Menéndez, and M. Cardona, Phys. Rev. B **35**, 2886 (1987).

[12]W. Kauschke and M. Cardona, Phys. Rev. B **33**, 5473 (1986).

[13]W. Kauschke, M. Cardona, and E. Bauser, Phys. Rev. B **35**, 8030 (1987).

[14]V. Gavrilenko, C. Trallero-Giner, and M. Cardona, Solid State Commun. **67**, 459 (1988).

[15]R. J. Elliot, Phys. Rev. **108**, 1384 (1957).

[16]G. E. Pikus and G. L. Bir, Fiz. Tverd. Tela (Leningrad) **1**, 154 (1959) [Sov. Phys.—Solid State **1**, 136 (1959)]; G. L. Bir and G. E. Pikus, *ibid.* **2**, 2287 (1960) [*ibid.* **2**, 2039 (1961)].

[17]L. D. Landau and E. M. Lifshitz, *Quantum Mechanics, Course of Theoretical Physics* (Pergamon, New York, 1977), Vol. 3.

[18]B. H. Bayramov, A. B. Gol'tsev, E. Käräjämäki, R. Laih, T. Levola, and V. V. Toporov, Fiz. Tverd. Tela (Leningrad) **25**, 1286 (1983) [Sov. Phys.—Solid State **25**, 739 (1983)].

[19]E. O. Kane, Phys. Rev. B **11**, 3850 (1975).

[20]D. D. Sell and P. Lawaetz, Phys. Rev. Lett. **26**, 311 (1971).

[21]T. Takizawa, J. Phys. Soc. Jpn. **52**, 1057 (1983).

[22]A. Blacha, H. Presting, and M. Cardona, Phys. Status Solidi B **126**, 11 (1984).

[23]W. Gordon, Ann. Phys. (Leipzig) **2**, 1031 (1929).

[24]*Higher Transcendental Functions,* edited by A. Erdélyi (McGraw-Hill, New York, 1953), Vol. 1.

[25]V. N. Bessolov, T. T. Dedegkaev, A. N. Efimov, N. F. Karlenki, and Yu. F. Yakovlev, Fiz. Tverd. Tela (Leningrad) **22**, 2834 (1980) [Sov. Phys.—Solid State **22**, 1652 (1980)].

[26]D. Lawaetz, D. Sc. thesis, The Technical University of Denmark, Lyngby, 1978.

[27]D. D. Sell, Phys. Rev. B **6**, 3750 (1972).

[28]We denote by x, y, z, x', and y' the [100], [010], [001], [110], and [$1\bar{1}0$] directions of the crystal, respectively.